# Data on a rat infection model to assess porous titanium implant coatings

Croes, M.; de Visser, H.; Meij, B. P.; Lietart, K.; van der Wal, B. C.H.; Vogely, H. C.; Fluit, A. C.; Boel, C. H.E.; Alblas, J.; Weinans, H.

**DOI**
10.1016/j.dib.2018.10.157

**Publication date**
2018

**Document Version**
Final published version

**Published in**
Data in Brief

Acta Biomaterialia 81 (2018) 315–327

Contents lists available at ScienceDirect

Acta Biomaterialia

journal homepage: www.elsevier.com/locate/actabiomat

Full length article

# Antibacterial and immunogenic behavior of silver coatings on additively manufactured porous titanium

M. Croes [a], S. Bakhshandeh [a], I.A.J. van Hengel [b], K. Lietaert [c,d], K.P.M. van Kessel [e], B. Pouran [a,b], B.C.H. van der Wal [a], H.C. Vogely [a], W. Van Hecke [f], A.C. Fluit [e], C.H.E. Boel [e], J. Alblas [a], A.A. Zadpoor [b], H. Weinans [a,b,g], S. Amin Yavari [a,*]

[a] Department of Orthopedics, University Medical Center Utrecht, Utrecht, The Netherlands
[b] Department of Biomechanical Engineering, Delft University of Technology, Delft, The Netherlands
[c] 3D Systems – LayerWise NV, Leuven, Belgium
[d] Department of Metallurgy and Materials Engineering, KU Leuven, Leuven, Belgium
[e] Department of Medical Microbiology, University Medical Center Utrecht, Utrecht, The Netherlands
[f] Department of Pathology, University Medical Center Utrecht, Utrecht, The Netherlands
[g] Department of Rheumatology, University Medical Center Utrecht, Utrecht, The Netherlands

ARTICLE INFO

*Article history:*
Received 19 July 2018
Received in revised form 30 August 2018
Accepted 26 September 2018
Available online 28 September 2018

*Keywords:*
Anti-bacterial coatings
Porous implants
Additive manufacturing
Hydrogels
Electrophoretic deposition
Osteomyelitis
Rat tibia model
Bone morphology

ABSTRACT

Implant-associated infections (IAI) are often recurrent, expensive to treat, and associated with high rates of morbidity, if not mortality. We biofunctionalized the surface of additively manufactured volume-porous titanium implants using electrophoretic deposition (EPD) as a way to eliminate the peri-operative bacterial load and prevent IAI. Chitosan-based (Ch) coatings were incorporated with different concentrations of silver (Ag) nanoparticles or vancomycin. A full-scale *in vitro* and *in vivo* study was then performed to evaluate the antibacterial, immunogenic, and osteogenic activity of the developed implants. *In vitro*, Ch + vancomycin or Ch + Ag coatings completely eliminated, or reduced the number of planktonic and adherent *Staphylococcus aureus* by up to 4 orders of magnitude, respectively. In an *in vivo* tibia intramedullary implant model, Ch + Ag coatings caused no adverse immune or bone response under aseptic conditions. Following *Staphylococcus aureus* inoculation, Ch + vancomycin coatings reduced the implant infection rate as compared to chitosan-only coatings. Ch + Ag implants did not demonstrate antibacterial effects *in vivo* and even aggravated infection-mediated bone remodeling including increased osteoclast formation and inflammation-induced new bone formation. As an explanation for the poor antibacterial activity of Ch + Ag implants, it was found that antibacterial Ag concentrations were cytotoxic for neutrophils, and that non-toxic Ag concentrations diminished their phagocytic activity. This study shows the potential of EPD coating to biofunctionalize porous titanium implants with different antibacterial agents. Using this method, Ag-based coatings seem inferior to antibiotic coatings, as their adverse effects on the normal immune response could cancel the direct antibacterial effects of Ag nanoparticles.

**Statement of Significance**

Implant-associated infections (IAI) are a clinical, societal, and economical burden. Surface biofunctionalization approaches can render complex metal implants with strong local antibacterial action. The antibacterial effects of inorganic materials such as silver nanoparticles (Ag NPs) are often highlighted under very confined conditions *in vitro*. As a novelty, this study also reports the antibacterial, immunogenic, and osteogenic activity of Ag NP-coated additively-manufactured titanium *in vivo*. Importantly, it was found that the developed coatings could impair the normal function of neutrophils, the most important phagocytic cells protecting us from IAI. Not surprisingly, the Ag NP-based coatings were outperformed by an antibiotic-based coating. This emphasizes the importance of also targeting implant immune-modulatory functions in future coating strategies against IAI.



* Corresponding author at: Department of Orthopedics, University Medical Center Utrecht, Rm G05.228, P.O. Box 85500, Utrecht 3508, GA, The Netherlands.
*E-mail address:* s.aminyavari@umcutrecht.nl (S. Amin Yavari).

https://doi.org/10.1016/j.actbio.2018.09.051
1742-7061/

## 1. Introduction

The use of various fixation devices or prosthetic joints in trauma and orthopedic surgery is associated with implant-associated infection (IAI) rates of 1–5% [1,2]. Persisting IAI could manifest as a complicated clinical scenario and a burden on the patient's quality of life, since complete implant removal is often needed to clear the infection [2]. Moreover, the economic burden of IAI is enormous [2]. For example, it is projected that the annual costs to treat peri-prosthetic joint infections alone will exceed $1.62 billion by 2020 in the US [3]. Given the increasing demand for orthopedic interventions, the growing number of immune-compromised patients with high susceptibility to bacterial infections, and the occurence of antibiotic-resistance microorgansims, IAIs are considered a serious clinical, societal, and economical burden [3,4].

The resistance of bacteria against the host immune system and antibiotics increases dramatically once a biofilm has been formed [2]. It is therefore essential to fully eradicate planktonic bacteria in the first few days following the operation to prevent early infection (<3 months postoperatively) [5]. As compared to systemic treatment, localized delivery of antibacterial drugs is more likely to ensure peri-implant concentrations to reach therapeutic levels, while avoiding adverse systemic effects [6]. This is of particular importance considering the widespread use of antibiotics and the emergence of drug-resistant bacteria [7]. To further diminish those concerns, alternatives to antibiotics should be explored. For instance, inorganic antibacterial agents or antimicrobial peptides are attractive options due to their broad-spectrum bactericidal activity [8–10].

Silver (Ag) is an antimicrobial agent which has been clinically applied even before the discovery of penicillin [11]. Currently, there are several commercially available products that use Ag for its bacterial killing effects, including wound dressings, crèmes, and catheter coatings [12]. To date, the widespread use of Ag in orthopedic implants has been hampered due to its known toxicity for eukaryotic cells, which could in turn affect osseointegration [13]. Several lines of evidence suggest that the size and shape of the Ag particles need to be fine-tuned to reduce the side effects while maximizing the antibacterial effects, and that Ag in the form of nanoparticles (NPs) has particularly strong bactericidal activity [12,14,15]. Moreover, there is evidence to support that the method of immobilization of Ag particles on the implant surface can enhance the cytocompatibility both *in vitro* and *in vivo* [16,17].

A number of systems for local antibacterial drug delivery are currently used in clinical practice, including polymethylmethacrylate (PMMA) bone cement supplemented with antibiotics and biodegradable polymers [18]. Methods such as plasma-surface modification techniques, sputtering, or sol-gel coatings are being investigated to more efficiently immobilize drugs onto the surface of various metallic implants for their localized action [16,19,20]. Electrophoretic deposition (EPD) is a particularly versatile technique to biofunctionalize metal implants, since it could be applied to a variety of prosthetic implants irrespective of the antibacterial agent or the complexity of the implant [21]. Additively-manufactured (AM) highly porous implants [22–24] are an emerging class of medical devices that could benefit from EPD biofunctionalization. AM porous Ti could be fine-tuned to facilitate osseointegration deep into the porous structure or to adjust the load-bearing conditions [25]. In addition, they could provide high porosity and a huge surface area available for coating, i.e. attachment of antibacterial agents [26].

We previously showed that EPD-based coatings laden with Ag NPs or antibiotics renders porous Ti implants with bactericidal activity *in vitro* [27,28]. Next, to account for the diverse pro-inflammatory and cytotoxic effects of Ag [29,30], it is of importance to evaluate the performance of such implants in a relevant bone model that captures the full spectrum of interactions between the antibacterial agent, immune cells, and bone cells. As such, it is possible that bacterial clearance by host immune cells is influenced by their interaction with Ag NPs [31]. In addition, local delivery of silver ions could have implications in terms of osseointegration through modulating the osteogenic response [32,33].

In the current study, we perform a full-scale study of the *in vitro* and *in vivo* performance of EPD-biofunctionalized AM porous Ti. To this end, we develop chitosan-based coatings containing Ag NPs or vancomycin. *In vitro*, the bacterial killing properties and the cytocompatibility for osteoblast-like cells and neutrophils of the implants is investigated. *In vivo*, septic and aseptic rat tibia models are used to evaluate the antibacterial, immunogenic and osteogenic performance of the developed biomaterials.

## 2. Materials and methods

### 2.1. Study design

Porous rod-shaped Ti implants were produced by direct metal printing (DMP), and are referred to as the 'as manufactured' (AsM) implants. EPD was used to coat these implants with a chitosan gel (Ch), either with or without various concentrations of $AgNO_3$ in the electrolyte (Ch + 1–100 mM Ag). Implants biofunctionalized with vancomycin-loaded chitosan coatings (Ch + Vanco) were used as a positive control for bacterial killing efficiency [28].

The *in vitro* antimicrobial effects of the implants were determined and evaluated after 24 h and 7 days following exposure to *Staphylococcus aureus* (*S. aureus*). The cytocompatibility of the implants was determined in terms of adhesion and proliferation of MG-63 osteoblast-like cells after 24 h and 7 days.

The *in vivo* inflammatory response and peri-implant bone changes were investigated for implants without (Ch, $n = 4$) or with the highest concentration Ag (Ch + 100 mM Ag, $n = 4$) following 28 day intramedullary implantation in the rat tibia ('biocompatibility study').

The *in vivo* antibacterial properties of the different implants were investigated following *S. aureus* challenge in an intramedullary rat tibia model ('infection study'). The day-28 bacterial load and peri-implant bone changes were studied for the following implant groups: AsM ($n = 5$), Ch ($n = 8$), Ch + 1 mM Ag ($n = 8$), Ch + 50 mM Ag ($n = 8$), Ch + 100 mM Ag ($n = 8$), Ch + Vanco ($n = 5$).

### 2.2. Additive manufacturing

Direct Metal Printing (DMP) was performed on a ProX DMP 320 machine (3D Systems, Leuven, Belgium) to produce volume-porous Ti implants. Magics (Materialise, Leuven, Belgium) and DMP control software were used for file preparation. The unit cell had a rhombic dodecahedron geometry and a size of 0.8 mm. Pure Ti powder was used with spherical shape and chemical composition according to ASTM F67 (Grade 1). The manufacturing process was executed under inert gas atmosphere with oxygen concentrations below 50 ppm. The implants were cleaned in demineralized water using ultrasound. The final rod-shape implants had a diameter of 1.1 mm and a total length of 15 mm (3 mm solid portion and a 12 mm porous portion), and were designed for intramedullary implantation in rat tibiae [Data in brief]. Based on microCT measurements ($n = 3$), the following parameters were calculated: strut thickness, 224 ± 71 μm; pore size, 216 ± 73 μm; porosity, 50 ± 5%. The implants were washed consecutively with aceton, ethanol and ultra-pure water (MilliQ, Merck Millipore, Burlington, MA). Implants were air-dried and sterilized by autoclave for experiments.

### 2.3. Electrophoretic deposition (EPD)

Two platinum meshes were employed as anodes, while the porous Ti implants served as the cathode placed in between the meshes with equal distance (± 1 cm). The electrolyte was prepared by mixing 0.5 mg/mL of chitosan solution (dissolved overnight) for 45 min with the relative concentrations of silver nitrate ($AgNO_3$) or vancomycin corresponding to the different experimental groups. The processing parameters were fine-tuned for the different concentrations of $AgNO_3$ and vancomycin in the electrolyte (conditions in Supplementary Table 1). The coated rods were gently rinsed with ultrapure water (MilliQ) and left to dry overnight at room temperature.

### 2.4. Surface characterization

A FEI (NovaNano, Hillsboro, OR) scanning electron microscope (SEM) was used to characterize the surface morphology of the biofunctionalized specimens. The chemical compositions on the surfaces were determined using an X-ray photoelectron spectroscopy (XPS) device equipped with an Al Kα x-ray source with 1486.6 eV energy (K-AlphaTM, Thermo Electron, Waltham, MA). The peak of the C1s (at 284.84 eV) was used as reference to determine all binding energies. The atomic percentage of all elements was obtained by normalizing the area of their corresponding peak with respect to the sum of the peaks of all elements. A SEM machine (JSM-IT100, JEOL, Tokyo Japan) equipped with an energy-disperse spectrometer (EDS) was used to visualize biofilm formation on the implant surface, quantify the chemical composition of the area around the histology specimens, and perform EDS mapping on the Ch + Ag samples.

### 2.5. $Ag^+$ measurement

To determine how much $Ag^+$ was incorporated in the chitosan layer after EPD, three samples from each group were dissolved in 5% (v/v) $H_2SO_4$ and 40% (v/v) $HNO_3$ at 60 °C, and the total amount of $Ag^+$ was determined by inductively coupled plasma mass spectroscopy (ICP-OES, iCAP6300 Duo Instrument, Waltham, MA).

The release of Ag ions ($Ag^+$) from the Ch + Ag coated rods was also measured by ICP-OES. Three samples from each group were immersed in 1 mL ultrapure water (MilliQ) and incubated at 37 °C. The water was sampled up to 14 days to measure the concentration of $Ag^+$. Nitric acid (10 μl/ml) was added to the collected samples to ionize all the silver particles in the solution.

### 2.6. Bacterial culture

*S. aureus* (American Type Culture Collection 49230, Manassas, VA) was used as pathogen. This strain was originally isolated from an osteomyelitis patient and has shown to cause chronic bone infection in rats [34]. The bacteria were grown as described in detail elsewhere [Data in brief]. On the day of surgery, the bacterial suspensions were extensively washed with PBS and resuspended to a concentration of $1 \times 10^6$ CFU/10 μl in PBS for *in vivo* injection.

### 2.7. In vitro antibacterial assay

The implants were incubated for 24 h at 37 °C on a shaker in a freshly cultured bacterial suspension at $OD_{600} = 0.001$ ($\pm 5 \times 10^5$ bacteria/mL). For the measurements at day 7, the implants were placed in PBS for 6 days before being transferred into the bacterial suspension. The number of planktonic bacteria was determined by plate counting using serial dilutions. To determine the number of adherent bacteria, the implants were rinsed three times in PBS, transferred to clean PBS and sonicated for 1 min. A sample of the suspension was drawn for plate counting in triplicate. The antibacterial rate of the implants was calculated as described before [27].

### 2.8. Animal experiment

The animal experiments were performed after approval of the local Ethics Committee for Animal Experimentation (Utrecht University, The Netherlands) and the Central Authority for Scientific Procedures on Animals (approved protocol AVD115002016445). A total of 84 male Sprague Dawley rats (14-week old, Charles River, L'Arbresle, France) were used for the experiments. The rats were housed in groups of three at the Central Laboratory Animal Institute (Utrecht University). Food and water was available *ad libitum*.

A pilot study with AsM implants showed that the establishment of persistent infection was dependent on the *S. aureus* strain [Data in brief]. Inoculation with $10^6$ CFU of strain ATCC 49230 resulted in bone and implant infection in 4/4 animals after 28 days and was therefore the condition used to study the antibacterial performance of the various experimental groups. The same surgical procedure was used [Data in brief].

### 2.9. MicroCT imaging

The tibiae were removed from the surrounding soft tissue using a sterile technique. MicroCT (Quantum FX; PerkinElmer, Waltham, MA) images were acquired with a tube voltage of 90 kV, a tube current of 180 mA, and a field of view of 10 mm. The images were represented as a stack of 2D TIFF images with a resolution of 20 μm. Analyses were performed with the BoneJ plugin (version 1.3.12) in ImageJ freeware version 1.48 (U.S. National Institutes of Health).

The implant and surrounding Ag particles were excluded from the dataset based on a global threshold. The proximal fusion point between tibia and fibula was used as an anatomical reference to cover the same bone area in all samples. An adaptive threshold was applied based on the mean local grayscale distribution to segment the bone. The total bone volume (BV) was determined for a total of 600 slices (1.2 cm) distal to the reference point. The peri-implant BV and cortical BV were measured for a total of 20 slices (0.4 mm) taken at 4 mm or 8 mm from the reference point, and referred to as the 'proximal' and 'distal' locations respectively. The peri-implant BV was defined as the volume of the bone tissue present within a region-of-interest (ROI) enclosed by the inner perimeter of the cortex, while the cortical BV was defined as the volume of the bone tissue found outside of this ROI. Cortical segmentation was performed to determine the bone porosity, which was defined as the fraction (%) of the BV within the total volume of the cortex after segmentation. The outer perimeter (mm) of the segmented cortex was measured as a sign of cortical expansion.

Osteomyelitis-specific bone changes were scored by two blinded observers (MC & BP) on the raw scans according to one of the following categories: 0 (no radiographic abnormalities), 1 (mild periosteal reaction and/or mild osteolysis), 2 (cortical thickening and/or evident osteolysis), 3 (extensive osteolysis with focal loss of cortex), 4 (loss of the cortical morphology).

### 2.10. Histological processing

For the biocompatibility study, the bone and implant were left intact and fixed in 4% (w/v) formaldehyde. Samples were dehydrated by an ethanol series and embedded in methyl methacrylate (MMA). Subsequently, 35 μm thick sections were cut (Leica sawing microtome, Nusslochh, Germany) from the proximal and distal peri-implant bone regions. For the infection study, a 1 cm thick cross-sectional bone sample was harvested from the most distal part of the implant with a sterilized saw blade (Dremel rotary

saw, Breda, The Netherlands). After formaldehyde fixation, the bone specimens were decalcified in 0.3 M ethylenediaminetetraacetic acid (EDTA), embedded in paraffin, and cut into 6 μm thick sections. A pathologist (WVH) scored the signs of active and chronic inflammation.

### 2.11. Determination of bacterial load

Bones were weighed and homogenized (Polytron PT3100; Kinetica Benelux, Best, The Netherlands) under sterile conditions. Serial dilutions were cultured on blood agar plates in triplicate. CFU were counted and normalized to the weight of the fragments (0.55 ± 0.11 g on average). CFU assessment on contralateral untreated tibiae never demonstrated colony formation, confirming localized infection at the site of contamination. The implants were rinsed three times and sonicated for 1 min in PBS. Subsequently, a sample was taken for CFU determination by plate counting.

### 2.12. Bone histomorphometry

MMA sections were stained with basic fuchsin and methylene blue to visualize the bone tissue. For quantification of peri-implant bone, stained sections were pseudo-colored in Adobe Photoshop CS6 (Adobe Systems, San Jose, CA) and the bone area was measured within a ROI, defined as a 1.3 mm Ø cylinder selected around the center of the 1.1 mm Ø implant. The peri-implant bone area was averaged for a proximal and distal tibial MMA section.

### 2.13. Neutrophil viability and phagocytosis assay

Human neutrophils were isolated from heparinized blood as described before [35]. The blood was obtained from healthy donors with informed consent and approval from the Medical Ethics Committee (University Medical Center Utrecht, approved protocol 07-125/C). To establish possible Ag toxicity, neutrophils were treated for 30 min with different concentrations $AgNO_3$ and the cell permeability for 1 μM 4′,6-diamidino-2-phenylindole (DAPI) was measured by flow cytometry (FACSVerse, BD, Franklin Lakes, NJ). A possible effect of Ag on bacterial phagocytosis was quantified by labeling *S. aureus* (American Type Culture Collection 49230) with 0.5 mg/mL fluorescein isothiocyanate (FITC) for 1 h at 4 °C. The bacteria were washed, adjusted to a concentration of 5 x $10^8$ CFU/mL, and incubated with neutrophils (ratio of 10 bacteria per neutrophil) in the presence or absence of $AgNO_3$. To enable efficient bacterial opsonization [36], experiments were performed in the presence of different concentrations human pooled serum (HPS). Mixtures were incubated for 15 min at 37 °C while shaking at 750 rpm in a round bottom microplate and fixed with 1% paraformaldehyde. Neutrophil-associated fluorescent bacteria (% FITC + neutrophils) were measured on a flow cytometer (FACSVerse, BD). Data were analyzed with FlowJo version 10.1 (FlowJo, LLC).

### 2.14. Statistical analysis

The biocompatibility study was not designed to statistically compare groups, instead an arbitrary sample size of 4 was chosen. A sample size calculation was performed for the infection study, with the bone CFU as the main outcome parameter. The mean and standard deviation was based a previous pilot using AsM implants as control [Data in brief]. Using a power of 80%, a standard deviation of 60%, an effect size of 90%, and an adjusted alpha for the different Ag groups that are compared to the Ch-only group, it was found that a sample size of 8 was needed.

SPSS version 20 (IBM, Chicago, IL, USA) was used for statistical analyses. One-way ANOVA with Bonferroni post-hoc correction was performed to compare group means. The non-parametric Mann-Whitney *U* test was performed when the Levene's test showed no homogeneity of the variance. A Fisher's exact test was performed to study the differences between the number of culture-positive samples. The two-tailed Spearman's correlation ($r_s$) was calculated to determine the relationship between the radiographic osteomyelitis score and the histological osteoclast count.

## 3. Results

### 3.1. Implant coatings

The presence of Ti as bulk material was confirmed in the AsM implants by the Ti 2p double peak at 459–465 eV (Fig. 1A). The peaks for C and N respectively at 285 and 400.5 eV were indicative of the presence of organic material in the form of the chitosan bulk material. In the Ch + vanco group, there was a slightly higher concentration of C, which could be attributed to the imide and amide groups present in vancomycin (Table 1). Successful production of Ag-coated implants was validated by the Ag 3d peak with subpeaks at 368 and 374 eV (Fig. 1A). Quantification of the atomic percentage of the elements showed increasing percentages of Ag for the 1, 50, and 100 mM Ag groups (Table 1).

SEM images showed 5–30 μm size remnant Ti powder after the DMP process in all groups (Fig. 1B). EDS mapping analysis confirmed the homogeneous distribution of Ag NPs (Fig. 1C), and also showed that the Ag layer was more prominent for increasing Ag concentrations in the electrolyte (Table 2). The average size of the particles was estimated to be 500–1000 nm in all groups based on the observed particle size disitribution (Supplementary Fig. 1).

### 3.2. $Ag^+$ loading and release

ICP-OES measurement showed that the total amount of $Ag^+$ incorporated in the Ch + 1 mM Ag, Ch + 50 mM Ag and Ch + 100 mM Ag groups was 2.91 ± 0.19, 579.21 ± 20.04 and 1688.82 ± 30.05 μg/sample, respectively. The rate of $Ag^+$ release from the Ch + Ag coated implants correlated with the Ag concentrations in the electrolytes and was highest on the first day (Fig. 1D). The cumulative $Ag^+$ release was the largest for Ch + 100 mM Ag implants, with a logarithmic release curve reaching plateau after 7 days. This suggests that most of the $Ag^+$ was released in the observed period.

### 3.3. In vitro antibacterial and cytotoxic properties

The Ch + 50 mM Ag and Ch + 100 mM Ag implants demonstrated killing of *S. aureus* both at 24 h (Fig. 2A) and day 7 (Fig. 2B) when compared to AsM or Ch-only groups. For both time points, the Ch + 50 mM Ag and Ch + 100 mM Ag conditions showed consistent 2-log and 3-log reductions in the implant-adherent *S. aureus*, respectively. Killing of planktonic *S. aureus* was stronger at day 7 (2–4 log reductions) than at 24 h (1 log reduction). The antibacterial rate for the Ch + 50 mM Ag and Ch + 100 mM Ag groups exceeded 99.9% (Supplementary Fig. 2). Complete killing of *S. aureus* was seen in the Ch + vanco group at both time points (Fig. 2A, 2B). Day 7 SEM images confirmed the dose-dependent inhibition of bacterial colony formation on the surface of Ch + Ag implants, and the absence of cocci on the Ch + vanco implants (Supplementary Fig. 3).

The qualitative live/dead assay did not show apparent differences in the adhesion and growth of osteoblast-like MG-63 cells on the Ch-only or Ch-vanco coated implants when compared to AsM implants (Supplementary Fig. 4). Following the same trend as seen for their bacterial killing properties, the Ch + Ag implants showed a dose-dependent reduction in the attachment of MG-63 cells after 24 h.

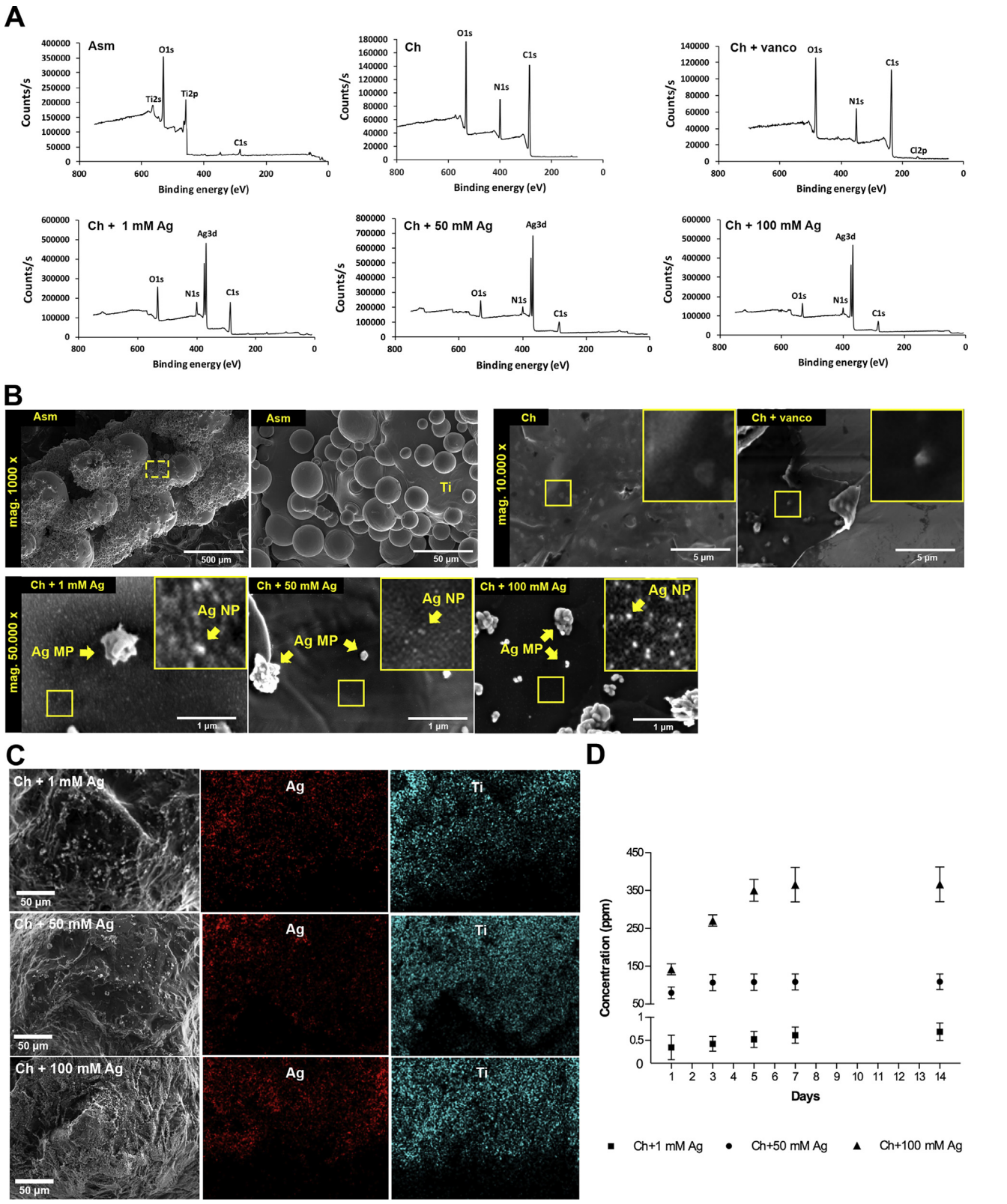


**Fig. 1.** Implant surface characterization. (A) XPS spectra showing the surface chemistry of the coatings. (B) Representative SEM images of the implant surfaces. Arrows indicate either Ag nanoparticles (NPs) or Ag microparticles (MPs). Asm, as manufactured; Ch, chitosan; Vanco, vancomycin; Ag, silver particles; Ti, titanium. (C) EDS mapping of the Ag-coated groups. (D) Cumulative $Ag^{+}$ release from Ch + Ag samples.

### 3.4. In vivo biocompatibility

At day 28 post-implantation, there were no signs of active inflammation on the surface or in the surrounding bone marrow of Ch-only or Ch + Ag implants surfaces (Fig. 3A). Fibrous capsule formation was seen in both groups, but was more prominent in the Ch + 100 mM Ag group. Deatched particles were seen around the Ch + 100 mM Ag implants, which were associated with

**Table 1**
Elemental composition of the implant coatings according to XPS.

| Group | Ti (%) | Ag (%) | C (%) | N (%) | O (%) | S/Fe/Na (%) |
|---|---|---|---|---|---|---|
| AsM | 23.42 | 0 | 13.22 | 3.43 | 46.72 | 13.23 |
| Ch | 0 | 0 | 55.26 | 13.58 | 20.06 | 11.1 |
| Ch + 1 mM Ag | 0 | 7.87 | 55.01 | 13.92 | 20.67 | 3.25 |
| Ch + 50 mM Ag | 0 | 15.36 | 39.99 | 19.48 | 17.76 | 7.41 |
| Ch + 100 mM Ag | 0 | 16.79 | 46.85 | 18.45 | 17.92 | 0 |
| Ch + vanco | 0 | 0 | 65.30 | 11.74 | 20.64 | 2.59 |

**Table 2**
EDS elemental analysis (At%) of the Ch + Ag implant coatings.

| Groups | Ti | C | N | O | Al | Ag |
|---|---|---|---|---|---|---|
| Ch + 1 mM Ag | 36.57 | 29.42 | 6.10 | 21.21 | 5.00 | 1.69 |
| Ch + 50 mM Ag | 46.08 | 19.76 | 5.81 | 20.95 | 2.57 | 4.82 |
| Ch + 100 mM Ag | 42.78 | 24.07 | 3.21 | 17.77 | 1.21 | 10.95 |

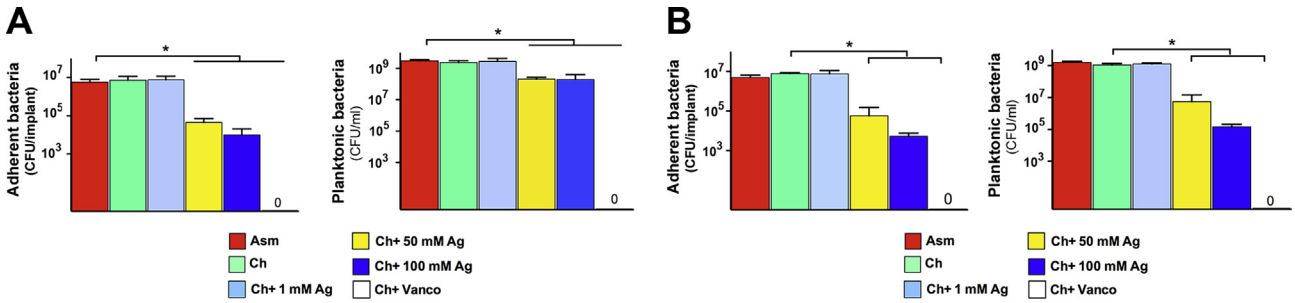


**Fig. 2.** *In vitro* antibacterial properties of EPD-coated implants. Adherent (left) and planktonic (right) colony-forming-unit (CFU) count after 24 h challenge of implants with *S. aureus*. (B) Implants incubated in PBS for 6 days were transferred into an *S. aureus* suspension. Histograms show the adherent (left) and planktonic (right) CFU count after 24 h bacterial challenge. Data are presented as mean ± SD ($n = 3$). $^{*}p < 0.05$; One-way ANOVA with Bonferroni post-hoc correction.

increased lymphocytic and monocytic cell infiltrates (Fig. 3A). EDS measurement showed that these particles were composed of C, N and Ag, and were therefore likely remnants of the Ch + Ag coating (Fig. 3B). Similar peri-implant bone formation was measured by histomorphometry in the Ch (0.12 ± 0.08 $mm^2$) and Ch + 100 mM Ag (0.09 ± 0.04 $mm^2$) groups. Cortical bone volume (Fig. 3C) and porosity (Fig. 3D) were comparable for both groups.

### 3.5. In vivo antibacterial effects

All bones (Fig. 4A) and implants (Fig. 4B) of the Ch-only and Ch + Ag groups were colonized with bacteria 28 days following bacterial inoculation. The Ch + Ag groups did not show any antibacterial effect as compared to the Ch-only group. There was a trend towards a decreased bone infection rate in the Ch + vanco group as compared to the Ch-only group (Fig. 4A). Moreover, a significant reduction ($p = 0.035$) in the number of culture-positive implants was found for the Ch + vanco group when compared to the Ch-only group (Fig. 4B).

In comparison to the prior study [Data in brief], there was a relatively large variation in the infection rate for AsM implants. Hence, we could not make a reliable comparison between the Ch-coated and AsM groups.

MicroCT quantification showed multiple signs of osteomyelitis in *S. aureus*-contaminated tibiae including periosteal new bone formation, thickening of the cortex, and osteolysis (Fig. 5A). The radiological signs of osteomyelitis were significantly higher in the Ch + 50 mM Ag ($p = 0.003$) and Ch + 100 mM Ag ($p = 0.0005$) groups than in the Ch-only group (Fig. 5B). A significant increase ($p = 0.003$) in the peri-implant bone mass in the Ch + 50 mM Ag and Ch + 100 mM Ag groups indicated a mixed catabolic and anabolic bone response (Fig. 5C). The cortical and peri-implant bone volume were quantified separately to better pinpoint the origin of the bone volume changes. While there were no changes in cortical bone volume between groups (Fig. 5D), the volume of peri-implant new bone was significantly higher in the Ch + 50 mM Ag and Ch + 100 mM Ag groups as compared to the Ch-only group (Fig. 5E). Conversely, there was a significantly reduced peri-implant bone in the Ch + vanco group. As a sign of cortical bone expansion, there was only a trend towards an increased bone perimeter in the Ch + Ag groups (Fig. 5F).

### 3.6. Histology

The soft tissues around the implants were characterized by the formation of fibrous capsules with monocyte/macrophage and lymphocyte infiltrations (Fig. 6A). There was a more pronounced fibrotic/chronic inflammatory reaction in the Ch-only and Ch + Ag groups, as indicated by the increased presence of myofibroblasts and the more prominent collagen deposition. In these fibrous capsules, neutrophils were only scarcely observed. In the Ch + 50 mM Ag and Ch + 100 mM Ag groups, pigment-laden macrophages were observed, suggesting the uptake of Ag particles. Normal-appearing bone marrow was seen further away from the implant in all groups. TRAP staining demonstrated an increased presence of osteoclasts due to infection (Fig. 6B). Among samples of the infection study, a trend was observed towards increased osteoclast numbers in Ch + Ag groups (Fig. 6C). In addition, there was a significant correlation ($r_s = 0.62$, $p < 0.0005$) between the histological osteoclast count and the microCT osteomyelitis score.

### 3.7. Neutrophil cell viability and phagocytosis

Short-term (30 min) exposure of neutrophils to Ag concentrations in the μM range strongly reduced their viability, with nearly complete killing of neutrophils following treatment with 10 μM Ag

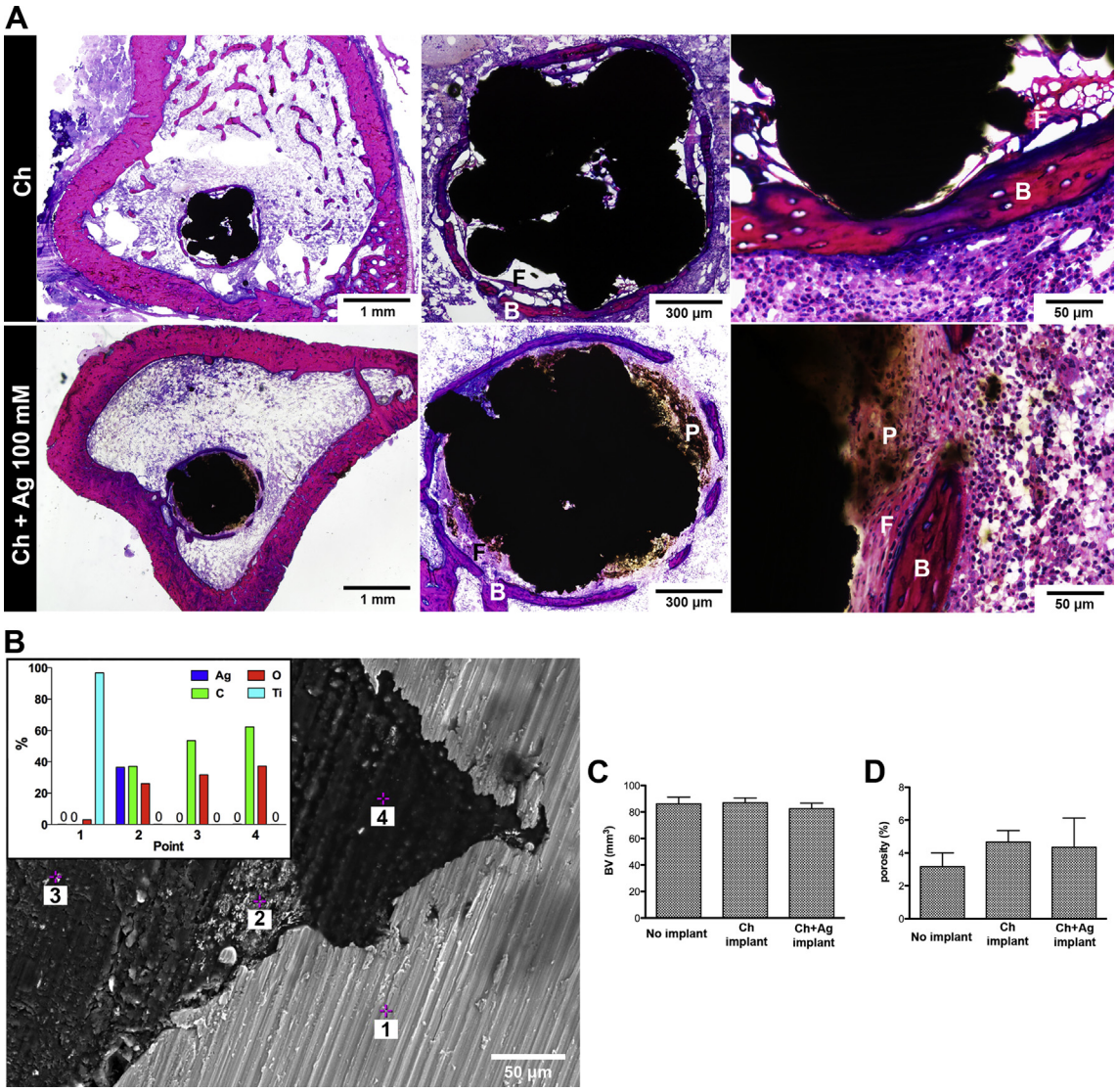


**Fig. 3.** *In vivo* biocompatibility of EPD-coated implants. (A) Basic fuchsin/methylene blue-stained MMA samples demonstrate peri-implant bone (B, pink), fibrous capsule (F) formation and presence of metallic particles (P) after 28 days implantation in the rat tibia. The images are representative for the group ($n = 4$). (B) EDX performed on MMA sections shows the different chemical compositions at the implant-tissue interface (300x magnification). (C, D) Day-28 microCT measurement of the cortical bone volume (C) and porosity (D) in contralateral tibiae without implant ($n = 6$) or tibiae receiving Chitosan-only (Ch, $n = 4$) or Chitosan + 100 mM Ag (Ch + Ag, $n = 4$) implants. (For interpretation of the references to colour in this figure legend, the reader is referred to the web version of this article.)

(Fig. 7A). For lower Ag concentrations, a significant reduction was seen in the neutrophil's capacity to phagocytose *S. aureus* (Fig. 7B). In the presence of 0.5% serum, Ag concentrations within the entire nM range reduced *S. aureus* uptake by up to 50%. A dose-dependent reduction in phagocytosis by Ag was apparent when experiments were performed using higher serum concentrations.

## 4. Discussion

Here, we demonstrated the suitability of EPD to surface-biofunctionalize implants and readily modify their properties in terms of *in vitro* cytocompatibility and antibacterial efficiency. Chitosan is a natural polymer, which is commonly used as a drug delivery vehicle on medical devices or tissue engineering scaffolds [37]. We found that chitosan is an effective EPD-based carrier to mediate antibacterial drug deposition onto porous Ti implants. The potential of EPD biofunctionalization was further addressed *in vitro* by showing that the chitosan-vancomycin coatings fully eradicated *S. aureus*, one of the most hazardous pathogens in IAI [2]. Chitosan + Ag implants induced up to 4-log reduction in planktonic and adherent *S. aureus*, and can therefore also be considered bactericidal [38]. At the same time, high Ag concentrations in the coatings were strongly cytotoxic for osteoblast-like cells. The toxicity of Ag NPs or the released Ag ions has often been reported, and is caused by the oxidative stress, DNA damage, and apoptosis [39]. In the current study, we observed a wide range of Ag nano- and microparticle sizes following Ch-based EPD (Supplementary Fig. 1). As the Ag particle size and associated dynamics of Ag ion release strongly influence Ag toxicity [39], future efforts should aim to define the ideal Ag NP coating with maximized bacterial killing and minimized host cell cytotoxicity. Equally important, the synergistic effect of Ag with other classes of antibacterial agents could be exploited to reduce Ag's toxicity and enhance its bacterial killing efficiency [9].

To evaluate whether the normal bone response towards porous Ti was disturbed by the immune modulatory or the cytotoxic effects of Ag [30,39], we evaluated the performance of chitosan-only and

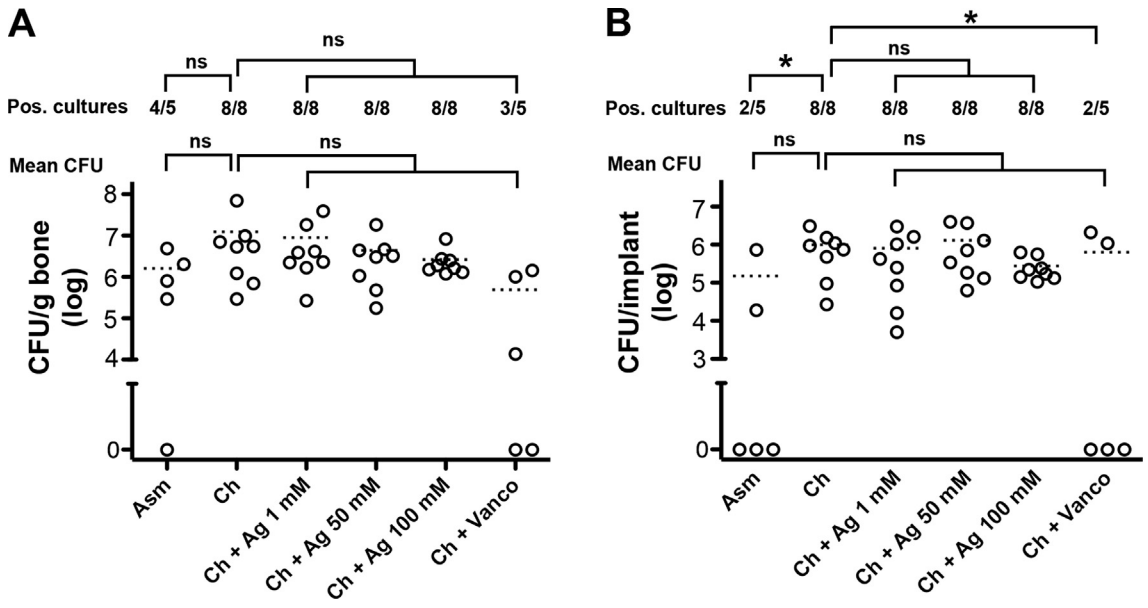


**Fig. 4.** *In vivo* antibacterial properties of EPD-coated implants. (A, B) Implants were implanted in the rat tibia following intramedullary contamination with $10^6$ colony-forming-units (CFU) *S. aureus*. The infection was quantified after 28 days with respect to the CFU in homogenized bone (A) and the CFU on the implant (B). The dotted lines indicate the group mean. $^*p < 0.05$; Fisher's exact test to assess differences in number of culture-positive samples. ns = not significant; One-way ANOVA with Bonferroni post-hoc correction to assess differences in mean CFU.

chitosan-Ag implants following 28-day implantation in the rat tibia. The sustained presence of Ag particles in the bone marrow in the chitosan-Ag group did not cause any obvious bone changes. Similarly, no active inflammation was observed at the endpoint of the study. This is in line with findings of others showing good short- and long-term osseointegration for Ag-coated implants manufactured through different techniques [40,41]. This suggests that, under appropriate conditions, the host regenerative capacity can overcome the cytotoxic effect of Ag. First, it is likely that the activity of osteoblast (progenitor) cells can restore after an initial burst release of Ag ions. Second, the *in vivo* performance of Ag-coated implants could be facilitated by pro-osteogenic effects of low concentrations of Ag [32]. To further strengthen the functionality of Ag-coated implants, follow-up studies should quantify the osseointegration by biomechanical tests or investigate their performance under load-bearing conditions.

The *in vivo* antibacterial effects of the EPD-biofunctionalized implants were investigated in an optimized rat osteomyelitis model. Due to its versatility and relatively low costs [42], the rat osteomyelitis model is an appropriate model to compare different coatings strategies, before testing the pre-clinical effectiveness with more clinically-relevant size implants in large animal species. Whereas all rats receiving chitosan-only implants established osteomyelitis as expected, there was an unexpected variation in the infection rate for uncoated implants [Data in brief]. Chitosan is generally thought to mitigate bacterial adhesion [43], and in agreement to other reports [44], we found that the chitosan increases the bactericidal effect of Ag *in vitro* (Supplementary Fig. 5). Moreover, the antibacterial rate of the Ch + Ag groups was more than 99% relative to the same implants without any coating. Therefore, it is unlikely that chitosan had promoted the development of infection in the rat model, although larger sample sizes are needed to be conclusively about this. Disregarding the fact that a direct comparison between uncoated implants and the different Ch-coated groups could not be made, EPD was shown to be a powerful tool to biofunctionalize porous implants with clinically applied antibiotics. In line with their *in vitro* bacterial killing capacity, the chitosan-vancomycin coatings significantly lowered the infection rate in comparison to the chitosan-only group, despite the challenging *S. aureus* inoculation dose chosen for this model [45]. To further guarantee full eradication of bacteria, combinatorial use of antimicrobial compounds seems a logical path to explore next.

The clinical use of Ag-coated implants is strongly debated. Whereas Ag-treated implants have shown safety in small patient populations [46], the routine use of Ag-coated implants has been hampered by a lack of evidence of antibacterial performance. In animal studies, Ag-coated orthopedic biomaterials demonstrate antibacterial effects in a subcutaneous location [47,48], whereas investigations in clinically-relevant bone models have yielded mostly dissappointing results [49,50]. Analogous to these previous reports, we found that Ag-coated implants failed to reduce the infection rate in our rat model. In fact, sustained Ag activity likely even further promoted the inflammatory response as shown by increased osteoclast formation and exaggerated bone remodeling. Although Ag particles were still detectable around the implants at day 28, their local distribution or the amount of released Ag ions apparently was insufficient to eradicate infection. A smarter approach may be needed to fully target the different routes leading to IAI. To illustrate, the simplified 'race for the surface' theory of implant infection as first termed by Gristina [51] is increasingly being challenged by evidence showing that bacteria largely reside within peri-implant tissue and cells [52]. If this is true, an ideal bactericidal coating may need the combination of firm Ag NP immobilization on the implant to prevent long-term bacterial adherence [16], together with immediate release of antibacterial agents in the surrounding tissue. In the same line of reasoning, combined delivery of Ag NPs and other classes of bactericidal agents carries potential to fully exploit the antibacterial effects of Ag NPs [28,53,54]. Finally, others have emphasized the role of the specific interaction between Ag NPs and serum proteins, which could affect the antimicrobial activity of Ag *in vivo* [55,56]. Therefore, the addition of human blood components or other biologically relevant compounds to the solutions may be a better *in vitro* model to test $Ag^+$ release behavior and toxicity for bacteria or eukaryotic cells.

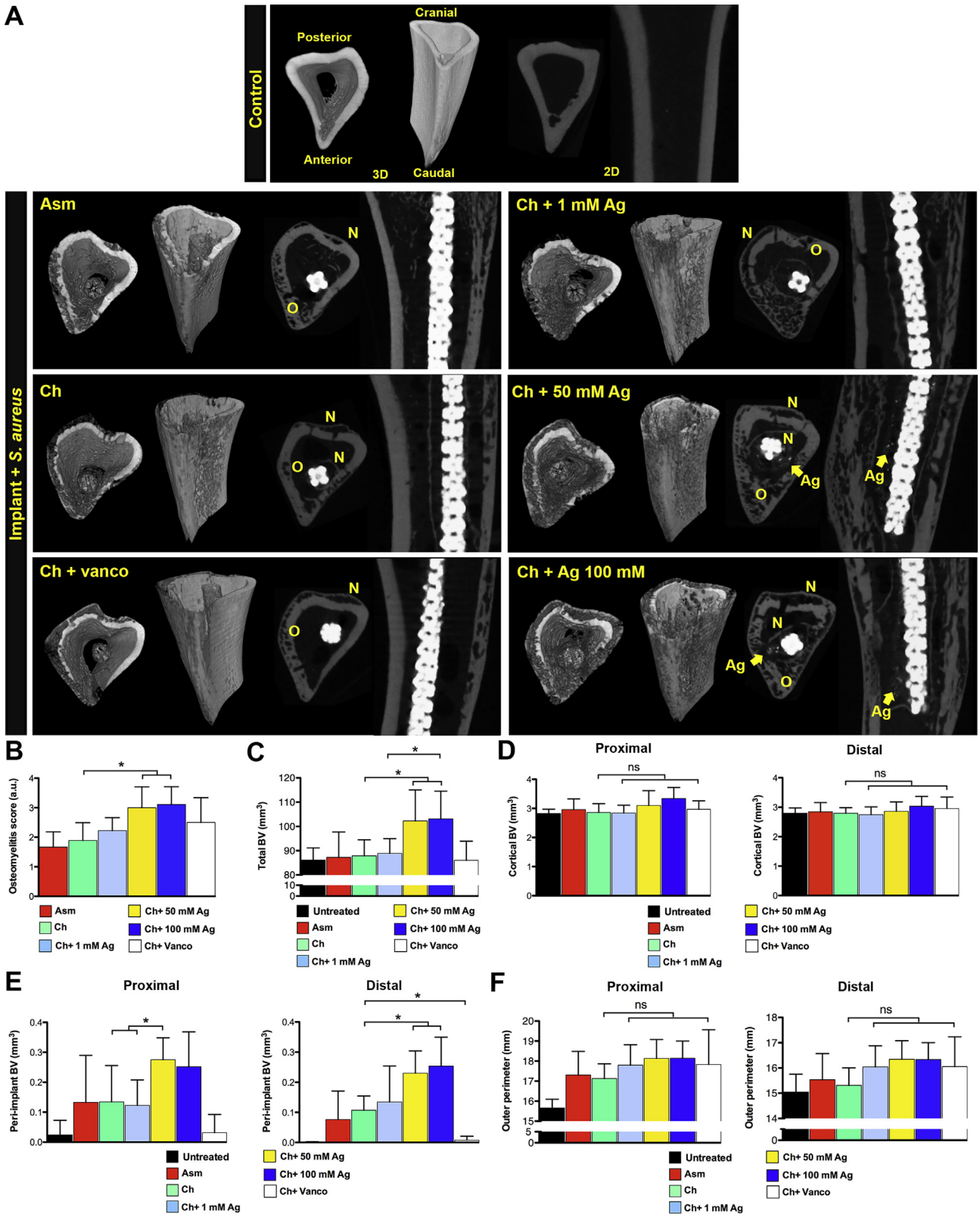


**Fig. 5.** Morphological bone changes in the infection study. EPD-coated implants were implanted in the rat tibia for 28 days following contamination with $10^6$ colony-forming-units (CFU) *S. aureus*. (A) Qualitative microCT image showing an untreated contralateral tibia (control) or *S. aureus*-contaminated tibiae receiving implants (Implant + *S. aureus*). Osteolysis (O) and new bone formation (N) were indicative of osteomyelitis. Images are representative for the group ($n$ = 6–9). (B) Radiological osteomyelitis score in *S. aureus*-contaminated tibiae: 0 = no radiographic abnormalities, 1 = mild periosteal reaction and/or mild osteolysis, 2 = cortical thickening and/or evident osteolysis, 3 = extensive osteolysis with focal loss of cortex, 4 = loss of cortical morphology. (C-F) The bone volume (C), cortical bone volume (D), peri-implant bone volume (E), outer cortical perimeter (F) were quantified by microCT in untreated contralateral tibia, or *S. aureus*-contaminated tibiae receiving different coated implants. Data are presented as mean ± SD ($n$ = 6–9). $^{*}p < 0.05$; One-way ANOVA (panels B, C, D, F) or Mann-Whitney $U$ test (panel E) with Bonferroni post-hoc correction. ns = not significant.

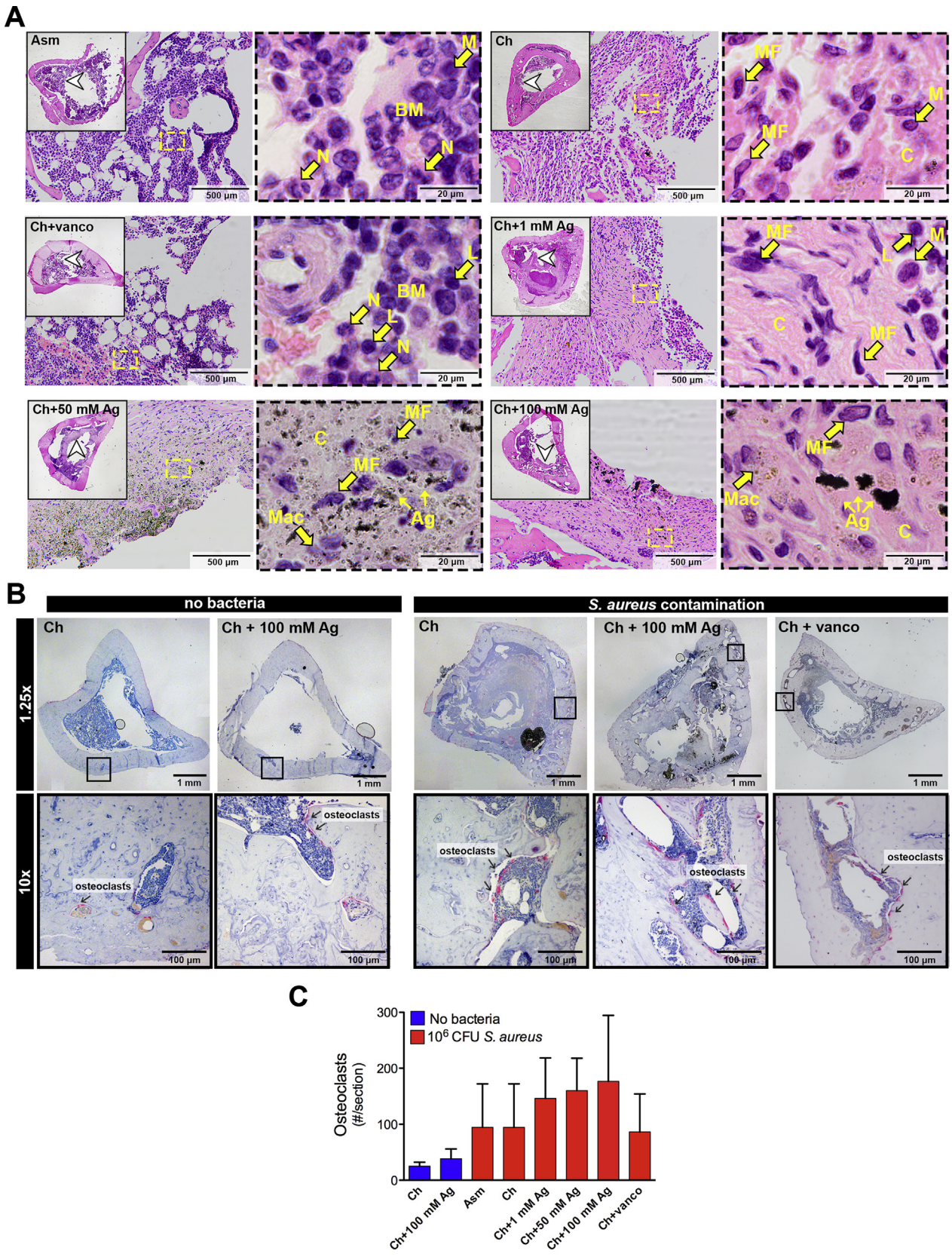


**Fig. 6.** Histological changes in the infection study. EPD-coated implants were implanted in the rat tibia for 28 days following contamination with $10^6$ colony-forming-units (CFU) *S. aureus*. (A) H&E staining showing the cellular composition in the peri-implant tissue. Images are representative for the group. (B) Staining for tartrate-resistant acid phosphatase (TRAP) activity to demonstrate the presence of osteoclasts in the aseptic tibia model (no bacteria) or the *S. aureus* infection model (*S. aureus* contamination). Mayer's hematoxylin was used as counterstain. (C) TRAP-positive cell count (mean ± SD) of samples from the aseptic tibia model (no bacteria, $n = 4$) or the *S. aureus* infection model ($10^6$ CFU *S. aureus*, $n = 5–8$). C = collagen fibers, BM = bone marrow, L = lymphocyte, M = monocyte, Mac = particle-laden macrophage, MF = myofibroblast, N = neutrophilic granulocyte.

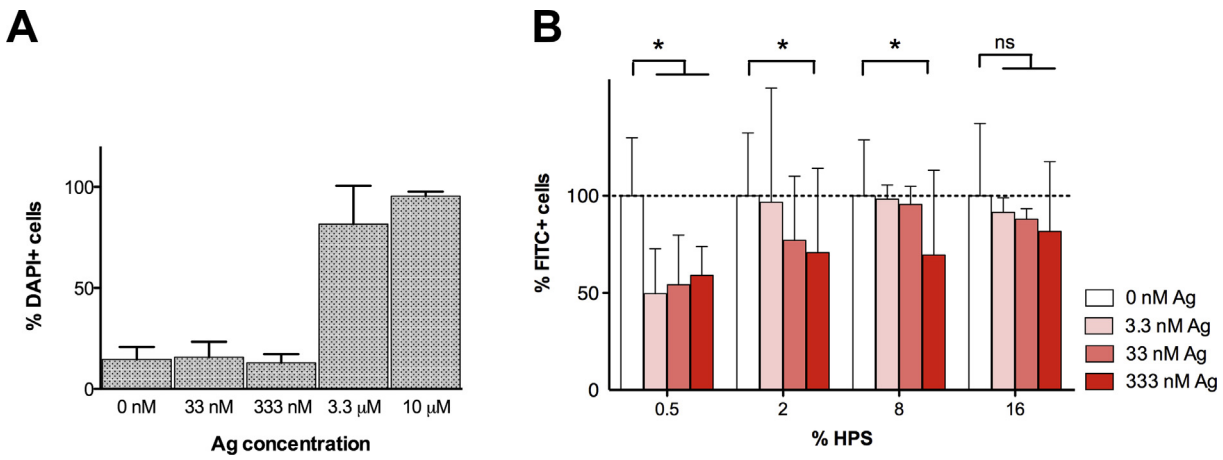


**Fig. 7.** Effect of Ag on human neutrophil viability and bacterial phagocytosis. (A) Percentage of non-viable neutrophils after 30 min incubation with $AgNO_3$ as measured by the flow cytometric DAPI uptake. Histogram shows the mean ± SD ($n = 2$ neutrophil donors). (B) Flow cytometric uptake of FITC-labeled *S. aureus* by neutrophils in the presence of different concentrations $AgNO_3$ and human pooled serum (HPS). Histograms show the mean ± SD ($n = 4–7$ neutrophil donors). $^{*}p < 0.05$; one-way repeated measures ANOVA with Bonferroni post-hoc correction. ns = not significant.

To further explain the poor bactericidal effects of Ag-based coatings in bone infection models, it is important to consider the different effects that Ag could have at the bone-implant interface, as shown schematically in Fig. 8. Similar to the different Ag particle sizes that were assembled by EPD, 0.1–1 μm size wear particles released from joint prosthesis are known to initiate an inflammatory cascade [57]. On the one hand, this could hamper the normal activity of phagocytes or suppress adaptive immunity [58–60]. On the other hand, the pro-inflammatory response to Ag likely explains why bones that received Ch + Ag implants were more severely affected than those receiving Ch-only implants, despite their similar bacterial load (Fig. 5, Fig. 6B). The inflammatory reaction to *S. aureus* infection is characterized by dynamic bone changes involving quiescent, resorbed and new bone [61]. Accordingly, the enhanced pro-inflammatory response in presence of high Ag concentrations can lead to an increased activity of bone forming cells and a net bone volume increase around the implant [61–64]. Moreover, increased osteoclast numbers in the Ch + Ag groups suggests that the presence of Ag led to further unwanted inflammation-induced osteoclastogenesis [65].

We furthermore hypothesized that the bactericidal effects of Ag NPs would come at the cost of impaired activity of phagocytic cells. Neutrophils form the first line of defense to infectious disease [66], and their important contribution in the anti-bacterial response is made clear by the fact that neutropenia leads to inability to clear infection [67]. From human neutrophil cultures in the current study we demonstrated that Ag strongly reduced neutrophil viability and phagocytic activity (Fig. 7). We propose that the detrimental effects of Ag NPs on neutrophil function have untill now been underestimated, which should not be overlooked in the development of novel antibacterial coatings.

Based on the above, the many actions of Ag around orthopedic implants can be considered a double-edged sword, for which the Ag feasibility depends on the specific clinical scenario. Since the host response could overcome the cytotoxic effect of Ag in the absence of infection (Fig. 3), it can also be reasoned that Ag may exert favorable antibacterial effects when there is a low bacterial challenge. However, when the body fails to eradicate infection, sustained Ag activity may mediate local hyper inflammation and kill neutrophils, which counteracts the general first defense immune response needed to fight the infection by the host.

The current study evaluated the *in vitro* and *in vivo* feasibility of applying EPD coatings to biofunctionalize AM porous implants for infection prevention. The developed implants rendered chitosan-vancomycin coating with antibacterial properties, which partially prevented infection in a challenging bone infection model. In contradiction to their direct *in vitro* bacterial killing effects, EPD-based chitosan-Ag implants did not prevent or reduce infection *in vivo*. Moreover, chitosan-Ag implants were found to negatively impact the bone response and the efficiency of bacterial uptake by innate immune cells. In conclusion, whereas antibiotic coating of AM implants by EPD is a promising strategy to combat IAI, caution should be exercised with the use of EPD-based Ag coatings, as Ag NPs can also have a negative impact on the innate immune response leading to persistent infection.

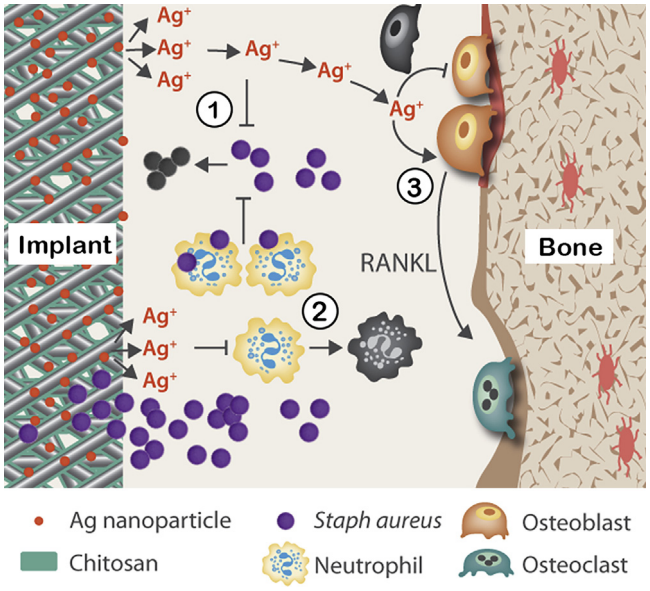


**Fig. 8.** Proposed mechanisms at the bone-implant interface by which Ag could affect implant osseointegration. 1. Ag nanoparticles release Ag ions that cause structural changes in bacterial cell walls and damage of bacterial proteins, DNA and RNA. This contributes to the antibacterial efficiency. 2. Ag particles or Ag ions induce the death of neutrophils through a direct mechanism. At the same time, sublethal Ag concentrations impair the phagocytic activity of neutrophils. This leads to decreased antibacterial efficiency. 3. In the presence of infection, Ag nanoparticles and/or Ag ions promote a hyper inflammatory reaction that causes an abnormal bone response, involving increased activity of bone-resorbing osteoclasts. Under sterile conditions, abnormal bone remodeling due to Ag nanoparticles of Ag ions is not observed.

## Acknowledgements

The research for this paper was financially supported by the Prosperos project, funded by the Interreg VA Flanders – The Netherlands program, CCI grant no. 2014TC16RFCB046. Dr. B.P. Meij (Clinical Sciences of Companion Animals, Utrecht University) and dr. H. de Visser are (Department of Orthopedics, University Medical Center Utrecht) gratefully thanked for their assistance during optimization of the rat model.

## Appendix A. Supplementary data

Supplementary data to this article can be found online at https://doi.org/10.1016/j.actbio.2018.09.051.

## References

[1] P.J. Marang-van de Mheen, E. Bragan Turner, S. Liew, N. Mutalima, T. Tran, S. Rasmussen, et al., Variation in Prosthetic Joint Infection and treatment strategies during 4.5 years of follow-up after primary joint arthroplasty using administrative data of 41397 patients across Australian, European and United States hospitals, BMC Musculoskelet Disord 18 (2017) 207.
[2] R.O. Darouiche, Treatment of infections associated with surgical implants, N. Engl. J. Med. 350 (2004) 1422–1429.
[3] S.M. Kurtz, E. Lau, H. Watson, J.K. Schmier, J. Parvizi, Economic burden of periprosthetic joint infection in the United States, J. Arthroplasty 27 (61–5) (2012) e1.
[4] A.J. Tande, R. Patel, Prosthetic joint infection, Clin. Microbiol. Rev. 27 (2014) 302–345.
[5] W. Zimmerli, A. Trampuz, P.E. Ochsner, Prosthetic-joint infections, N. Engl. J. Med. 351 (2004) 1645–1654.
[6] G.J. ter Boo, D.W. Grijpma, T.F. Moriarty, R.G. Richards, D. Eglin, Antimicrobial delivery systems for local infection prophylaxis in orthopedic- and trauma surgery, Biomaterials 52 (2015) 113–125.
[7] B. Spellberg, J.G. Bartlett, D.N. Gilbert, The future of antibiotics and resistance, N. Engl. J. Med. 368 (2013) 299–302.
[8] C.D. Fjell, J.A. Hiss, R.E. Hancock, G. Schneider, Designing antimicrobial peptides: form follows function, Nat Rev Drug Discov. 11 (2011) 37–51.
[9] J. Raphel, M. Holodniy, S.B. Goodman, S.C. Heilshorn, Multifunctional coatings to simultaneously promote osseointegration and prevent infection of orthopaedic implants, Biomaterials 84 (2016) 301–314.
[10] S.K. Nandi, A. Shivaram, S. Bose, A. Bandyopadhyay, Silver nanoparticle deposited implants to treat osteomyelitis, J. Biomed. Mater. Res. B Appl. Biomater. 106 (2018) 1073–1083.
[11] I. Chopra, The increasing use of silver-based products as antimicrobial agents: a useful development or a cause for concern?, J Antimicrob. Chemother. 59 (2007) 587–590.
[12] M. Rai, A. Yadav, A. Gade, Silver nanoparticles as a new generation of antimicrobials, Biotechnol. Adv. 27 (2009) 76–83.
[13] K. Mijnendonckx, N. Leys, J. Mahillon, S. Silver, R. Van Houdt, Antimicrobial silver: uses, toxicity and potential for resistance, Biometals 26 (2013) 609–621.
[14] G.A. Sotiriou, S.E. Pratsinis, Antibacterial activity of nanosilver ions and particles, Environ. Sci. Technol. 44 (2010) 5649–5654.
[15] S. Pal, Y.K. Tak, J.M. Song, Does the antibacterial activity of silver nanoparticles depend on the shape of the nanoparticle? A study of the Gram-negative bacterium Escherichia coli, Appl. Environ. Microbiol. 73 (2007) 1712–1720.
[16] H. Qin, H. Cao, Y. Zhao, C. Zhu, T. Cheng, Q. Wang, et al., In vitro and in vivo anti-biofilm effects of silver nanoparticles immobilized on titanium, Biomaterials 35 (2014) 9114–9125.
[17] I.A.J. van Hengel, M. Riool, L.E. Fratila-Apachitei, J. Witte-Bouma, E. Farrell, A.A. Zadpoor, et al., Selective laser melting porous metallic implants with immobilized silver nanoparticles kill and prevent biofilm formation by methicillin-resistant Staphylococcus aureus, Biomaterials 140 (2017) 1–15.
[18] J.S. Gogia, J.P. Meehan, P.E. Di Cesare, A.A. Jamali, Local antibiotic therapy in osteomyelitis, Semin Plast Surg. 23 (2009) 100–107.
[19] M.A. Massa, C. Covarrubias, M. Bittner, I.A. Fuentevilla, P. Capetillo, A. Von Marttens, et al., Synthesis of new antibacterial composite coating for titanium based on highly ordered nanoporous silica and silver nanoparticles, Mater. Sci. Eng. C Mater. Biol. Appl. 45 (2014) 146–153.
[20] M.A. Ur Rehman, S. Ferraris, W.H. Goldmann, S. Perero, F.E. Bastan, Q. Nawaz, et al., Antibacterial and bioactive coatings based on radio frequency Co-sputtering of silver nanocluster-silica coatings on peek/bioactive glass layers obtained by electrophoretic deposition, ACS Appl. Mater. Interfaces 9 (2017) 32489–32497.
[21] S. Bakhshandeh, Yavari S. Amin, Electrophoretic deposition: a versatile tool against biomaterial associated infections, J. Mater. Chem. B 6 (2018) 1128–1148.
[22] Z. Gorgin Karaji, M. Speirs, S. Dadbakhsh, J.P. Kruth, H. Weinans, A.A. Zadpoor, et al., Additively manufactured and surface biofunctionalized porous nitinol, ACS Appl. Mater. Interfaces 9 (2017) 1293–1304.
[23] A.A. Zadpoor, J. Malda, Additive manufacturing of biomaterials, tissues, and organs, Ann. Biomed. Eng. 45 (2017) 1–11.
[24] J. van der Stok, M.K. Koolen, M.P. de Maat, S.A. Yavari, J. Alblas, P. Patka, et al., Full regeneration of segmental bone defects using porous titanium implants loaded with BMP-2 containing fibrin gels, Eur. Cells Mater. 29 (2015) 141–153. discussion 53-4.
[25] F.S.L. Bobbert, K. Lietaert, A.A. Eftekhari, B. Pouran, S.M. Ahmadi, H. Weinans, et al., Additively manufactured metallic porous biomaterials based on minimal surfaces: a unique combination of topological, mechanical, and mass transport properties, Acta Biomater. 53 (2017) 572–584.
[26] S. Amin Yavari, S.M. Ahmadi, J. van der Stok, R. Wauthle, A.C. Riemslag, M. Janssen, et al., Effects of bio-functionalizing surface treatments on the mechanical behavior of open porous titanium biomaterials, J. Mech. Behav. Biomed. Mater. 36 (2014) 109–119.
[27] S. Amin Yavari, L. Loozen, F.L. Paganelli, S. Bakhshandeh, K. Lietaert, J.A. Groot, et al., Antibacterial behavior of additively manufactured porous titanium with nanotubular surfaces releasing silver ions, ACS Appl. Mater. Interfaces 8 (2016) 17080–17089.
[28] S. Bakhshandeh, Z. Gorgin Karaji, K. Lietaert, A.C. Fluit, C.H.E. Boel, H.C. Vogely, et al., Simultaneous delivery of multiple antibacterial agents from additively manufactured porous biomaterials to fully eradicate planktonic and adherent staphylococcus aureus, ACS Appl. Mater. Interfaces 9 (2017) 25691–25699.
[29] A. Murphy, A. Casey, G. Byrne, G. Chambers, O. Howe, Silver nanoparticles induce pro-inflammatory gene expression and inflammasome activation in human monocytes, J. Appl. Toxicol. 36 (2016) 1311–1320.
[30] J. Park, D.H. Lim, H.J. Lim, T. Kwon, J.S. Choi, S. Jeong, et al., Size dependent macrophage responses and toxicological effects of Ag nanoparticles, Chem. Commun. (Camb.) 47 (2011) 4382–4384.
[31] H. Haase, A. Fahmi, B. Mahltig, Impact of silver nanoparticles and silver ions on innate immune cells, J. Biomed. Nanotechnol. 10 (2014) 1146–1156.
[32] R. Zhang, P. Lee, V.C. Lui, Y. Chen, X. Liu, C.N. Lok, et al., Silver nanoparticles promote osteogenesis of mesenchymal stem cells and improve bone fracture healing in osteogenesis mechanism mouse model, Nanomedicine 11 (2015) 1949–1959.
[33] S. Castiglioni, A. Cazzaniga, L. Locatelli, J.A.M. Maier, Silver nanoparticles in orthopedic applications: new insights on their effects on osteogenic cells, Nanomaterials (Basel) (2017;7.).
[34] M. Lucke, G. Schmidmaier, S. Sadoni, B. Wildemann, R. Schiller, A. Stemberger, et al., A new model of implant-related osteomyelitis in rats, J. Biomed. Mater. Res. B Appl. Biomater. 67 (2003) 593–602.
[35] C. Prat, J. Bestebroer, C.J. de Haas, J.A. van Strijp, K.P. van Kessel, A new staphylococcal anti-inflammatory protein that antagonizes the formyl peptide receptor-like 1, J. Immunol. 177 (2006) 8017–8026.
[36] K.P. van Kessel, J. Bestebroer, J.A. van Strijp, Neutrophil-Mediated Phagocytosis of Staphylococcus aureus, Front. Immunol. 5 (2014) 467.
[37] A. Di Martino, M. Sittinger, M.V. Risbud, Chitosan: a versatile biopolymer for orthopaedic tissue-engineering, Biomaterials 26 (2005) 5983–5990.
[38] G.A. Pankey, L.D. Sabath, Clinical relevance of bacteriostatic versus bactericidal mechanisms of action in the treatment of Gram-positive bacterial infections, Clin. Infect. Dis. 38 (2004) 864–870.
[39] S. Kim, D.Y. Ryu, Silver nanoparticle-induced oxidative stress, genotoxicity and apoptosis in cultured cells and animal tissues, J. Appl. Toxicol. 33 (2013) 78–89.
[40] A. Shivaram, S. Bose, A. Bandyopadhyay, Understanding long-term silver release from surface modified porous titanium implants, Acta Biomater. 58 (2017) 550–560.
[41] C. Gao, Y. Wang, F. Han, Z. Yuan, Q. Li, C. Shi, et al., Antibacterial activity and osseointegration of silver-coated poly(ether ether ketone) prepared using the polydopamine-assisted deposition technique, J. Mater. Chem. B 5 (2017) 9326–9336.
[42] W. Reizner, J.G. Hunter, N.T. O'Malley, R.D. Southgate, E.M. Schwarz, S.L. Kates, A systematic review of animal models for Staphylococcus aureus osteomyelitis, Eur. Cells Mater. 27 (2014) 196–212.
[43] D. Raafat, K. von Bargen, A. Haas, H.G. Sahl, Insights into the mode of action of chitosan as an antibacterial compound, Appl. Environ. Microbiol. 74 (2008) 3764–3773.
[44] M. Potara, E. Jakab, A. Damert, O. Popescu, V. Canpean, S. Astilean, Synergistic antibacterial activity of chitosan-silver nanocomposites on Staphylococcus aureus, Nanotechnology 22 (2011) 135101.
[45] B. Friberg, S. Friberg, L.G. Burman, Inconsistent correlation between aerobic bacterial surface and air counts in operating rooms with ultra clean laminar air flows: proposal of a new bacteriological standard for surface contamination, J. Hosp. Infect. 42 (1999) 287–293.
[46] F. Donati, G. Di Giacomo, S. D'Adamio, A. Ziranu, S. Careri, M. Rosa, et al., Silver-coated hip megaprosthesis in oncological limb savage surgery, Biomed Res. Int. 2016 (2016) 9079041.
[47] R. Kuehl, P.S. Brunetto, A.K. Woischnig, M. Varisco, Z. Rajacic, J. Vosbeck, et al., Preventing implant-associated infections by silver coating, Antimicrob. Agents Chemother. 60 (2016) 2467–2475.
[48] T. Shimazaki, H. Miyamoto, Y. Ando, I. Noda, Y. Yonekura, S. Kawano, et al., In vivo antibacterial and silver-releasing properties of novel thermal sprayed silver-containing hydroxyapatite coating, J. Biomed. Mater. Res. B Appl. Biomater. 92 (2010) 386–389.
[49] T. Akiyama, H. Miyamoto, Y. Yonekura, M. Tsukamoto, Y. Ando, I. Noda, et al., Silver oxide-containing hydroxyapatite coating has in vivo antibacterial activity in the rat tibia, J. Orthop. Res. 31 (2013) 1195–1200.

[50] E. Sheehan, J. McKenna, K.J. Mulhall, P. Marks, D. McCormack, Adhesion of Staphylococcus to orthopaedic metals, an in vivo study, J. Orthop. Res. 22 (2004) 39–43.
[51] A.G. Gristina, Biomaterial-centered infection: microbial adhesion versus tissue integration, Science 237 (1987) 1588–1595.
[52] M. Riool, L. de Boer, V. Jaspers, C.M. van der Loos, W.J.B. van Wamel, G. Wu, et al., Staphylococcus epidermidis originating from titanium implants infects surrounding tissue and immune cells, Acta Biomater. 10 (2014) 5202–5212.
[53] H. Deng, D. McShan, Y. Zhang, S.S. Sinha, Z. Arslan, P.C. Ray, et al., Mechanistic study of the synergistic antibacterial activity of combined silver nanoparticles and common antibiotics, Environ. Sci. Technol. 50 (2016) 8840–8848.
[54] M. Lu, J. Liao, J. Dong, J. Wu, H. Qiu, X. Zhou, et al., An effective treatment of experimental osteomyelitis using the antimicrobial titanium/silver-containing nHP66 (nano-hydroxyapatite/polyamide-66) nanoscaffold biomaterials, Sci. Rep. 6 (2016) 39174.
[55] D.P. Gnanadhas, M. Ben Thomas, R. Thomas, A.M. Raichur, D. Chakravortty, Interaction of silver nanoparticles with serum proteins affects their antimicrobial activity in vivo, Antimicrob. Agents Chemother. 57 (2013) 4945–4955.
[56] G. Mulley, A.T. Jenkins, N.R. Waterfield, Inactivation of the antibacterial and cytotoxic properties of silver ions by biologically relevant compounds, PLoS One 9 (2014) e94409.
[57] E. Ingham, J. Fisher, The role of macrophages in osteolysis of total joint replacement, Biomaterials 26 (2005) 1271–1286.
[58] M. Benoit, B. Desnues, J.L. Mege, Macrophage polarization in bacterial infections, J. Immunol. 181 (2008) 3733–3739.
[59] A.H. Hosman, H.C. van der Mei, S.K. Bulstra, H.J. Busscher, D. Neut, Effects of metal-on-metal wear on the host immune system and infection in hip arthroplasty, Acta Orthop. 81 (2010) 526–534.
[60] X. Miao, X. Leng, Q. Zhang, The current state of nanoparticle-induced macrophage polarization and reprogramming research, Int. J. Mol. Sci. 18 (2017).
[61] V.A. Stadelmann, I. Potapova, K. Camenisch, D. Nehrbass, R.G. Richards, T.F. Moriarty, In vivo MicroCT monitoring of osteomyelitis in a rat model, Biomed Res. Int. 2015 (2015) 587857.
[62] G. Mbalaviele, D.V. Novack, G. Schett, S.L. Teitelbaum, Inflammatory osteolysis: a conspiracy against bone, J Clin Invest. 127 (2017) 2030–2039.
[63] M. Croes, W. Boot, M.C. Kruyt, H. Weinans, B. Pouran, Y.J.M. van der Helm, et al., Inflammation-induced osteogenesis in a rabbit tibia model, Tissue Eng. Part C Methods 23 (2017) 673–685.
[64] M. Croes, M.C. Kruyt, L. Loozen, A.H. Kragten, H. Yuan, W.J. Dhert, et al., Local induction of inflammation affects bone formation, Eur. Cells Mater. 33 (2017) 211–226.
[65] M.C. Walsh, N. Takegahara, H. Kim, Y. Choi, Updating osteoimmunology: regulation of bone cells by innate and adaptive immunity, Nat. Rev. Rheumatol. 14 (2018) 146–156.
[66] Y. Li, A. Karlin, J.D. Loike, S.C. Silverstein, A critical concentration of neutrophils is required for effective bacterial killing in suspension, Proc. Natl. Acad. Sci. U. S.A. 99 (2002) 8289–8294.
[67] D. Pletzer, S.C. Mansour, K. Wuerth, N. Rahanjam, R.E. Hancock, New mouse model for chronic infections by gram-negative bacteria enabling the study of anti-infective efficacy and host-microbe interactions, MBio. 8 (2017).